CICE 2023 Rio de Janeiro - Brazil 11TH INTERNATIONAL CONFERENCE ON FRP COMPOSITES IN CIVIL ENGINEERING

BOND BEHAVIOUR OF A STICK SHAPE CFRP REINFORCEMENT APPLIED ACCORDING TO THE NSM-ETS STRENGTHENING TECHNIQUES

Luís Correia, ISISE/ ARISE, University of Minho, Portugal, lcorreia@civil.uminho.pt
Joaquim Barros, ISISE/ ARISE, University of Minho, Portugal, jbarros@civil.uminho.pt
Pedram Ayyobi, ISISE/ ARISE, University of Minho, Portugal, pedram.ayyobi@gmail.com
Hossein Malekinejad, ISISE/ ARISE, University of Minho, Portugal, hmalekinejad68@gmail.com

ABSTRACT
This paper investigates a hybrid strengthening technique that combines the near-surface-mounted (NSM) technique for flexural strengthening with the embedded through section (ETS) technique for shear strengthening using innovative stick-shaped CFRP rebars. The study focuses on the mechanical properties and bond behavior of 7 mm square-sectioned, 30°-bent CFRP rebars. The mechanical characteristics and bond behavior were evaluated by tensile testing, interlaminar shear tests, and direct pull-out tests. The results of the pull-out tests revealed FRP failure, showing a strong link between concrete and CFRP. The findings illustrate the efficiency of the hybrid NSM-ETS technique for reinforcing structures using stick-shaped CFRP laminates.

KEYWORDS
Bond behavior, hybrid NSM-ETS, mechanical properties, pull-out tests.

INTRODUCTION

The occurrence of premature failure modes, such as concrete cover separation or rip-off failure, has impeded the efficiency of CFRP reinforcements placed using the NSM technique for flexural strengthening (J. A. O. Barros & Fortes, 2005; Teng et al., 2006). Wrapping the end extremities of NSM reinforcements with U-shaped CFRP wet layup strips provides RC beams with both flexural and shear reinforcement (Dias et al., 2021). However, this strategy comes with additional costs and is not applicable in the case of RC slabs. An alternative approach involves the use of FRP reinforcement with a bent extremity inserted through the section (ETS) technique, which appears to be less susceptible to fire damage and can provide residual strengthening effects (Firmo et al., 2015). These bent extremities prevent rip-off failures by providing ideal anchorage conditions to the NSM-applied reinforcement and, depending on their inclination and anchorage length, contribute to the shear capacity of RC beams (J. A. O. Barros et al., 2017; Imjai et al., 2020). FRP bars applied using the NSM and ETS techniques have also shown efficient shear and flexural strengthening capabilities in RC beams (J. Barros et al., 2016; Chalioris et al., 2018; Kaya et al., 2017).

Prefabricated pultruded CFRP laminates with rectangular cross-sections, thermally transformed to have one or two inclined extremities (clip or sticker configuration), have been successfully employed for simultaneous flexural and punching strengthening of RC slabs (J. A. O. Barros et al., 2017, 2022). These laminates consist of one part applied using the NSM technique and one or more parts applied with the ETS technique, joined by a transition zone that reshapes the rectangular cross-section into a nearly circular form. Pullout tests conducted on the first generation of these CFRP reinforcements (known as CutInov) revealed premature failure in the transition zone as a result of the relatively low tensile strength resulting from the thermo-mechanical post-treatment used to achieve the desired inclination of the extremities. This branch of the CFRP reinforcement is subjected to a multiaxial stress field (axial, bending, and shear forces), which contributes to the anticipation of its rupture (Carlos Augusto Nonato da Silva, 2019; Nonato Da Silva et al., 2019).

Subsequent developments have led to the creation of new generations of CutInov CFRP bars (J. A. O. Barros et al., 2022). Although improvements have been made, the transition zone is still the weekest part of this reinforcement. Nonetheless, promising results have been observed in real-scale structures (J. A. O. Barros et al., 2017, 2022), particularly in cantilever beams where the anchorage conditions of the ETS part of the CFRP bar limit the strengthening intervention to the balcony's cantilever zone, minimizing intrusion into the building's interior.

This study presents preliminary experimental test results on a new generation of CFRP bars produced using vacuum infusion, featuring a 30º angle between the inclined and horizontal parts of the FRP reinforcement. The CFRP bar underwent mechanical characterization through tensile tests, followed by direct pull-out tests using three different bond lengths to assess its bond performance with concrete. The bond of this bar was assured using a fluid epoxy adhesive. In some specimens, premature failures occurred, prompting further investigation into the interlaminar shear strength of the composite material.

EXPERIMENTAL PROGRAM

This study was conducted as part of the research project titled "StickeR: Innovative Technique for Structural Reinforcement Based on CFRP Laminates of Multifunctional Requirements and Applied with Advanced Cement Matrix Adhesive" (POCI-01-0247-FEDER-039755). The project aimed to investigate the structural advantages of a novel CFRP bar geometry, which is installed using the near-surface-mounted (NSM) and embedded through section (ETS) techniques, with the potential to enhance flexural capacity, punching shear capacity, shear capacity, and mitigate rip-off failure.

The project encompassed multiple aspects, including the development of the composite material, enhancement of the installation technique, and evaluation of the structural behavior of this composite material when applied to real-scale structures such as beams and slabs. Additionally, direct pull-out tests were conducted to further examine the performance of the composite material.

Through this research project, the structural benefits and potential applications of the new CFRP bar geometry in reinforced structures was sought, aiming to contribute to the advancement of the field and provide innovative solutions for structural reinforcement.

Direct pull-out tests

Specimens geometry and preparation

The experimental program included 18 direct pull-out tests. In each direct pull-out test, a single CFRP rebar was adhesively bonded to a concrete prism. The concrete prism featured a squared cross-section, measuring 150 mm in width. The length of the concrete prisms varied, with specimens measuring 200 mm, 300 mm, or 400 mm in length. The purpose of these tests was to assess the bond strength between the CFRP rebar and the concrete matrix. To create the CFRP rebars, a vacuum infusion technique was employed. This involved the use of 1000g/m^2 sheets of carbon fiber, which were carefully infused with a resin matrix to create a 7 mm thick plate (CFRP thickness, t_f, was 7mm). Subsequently, the cured composite plate was accurately cut into individual CFRP rebars with a cross-section, measuring 7 mm in width. The specimens preparation followed the same steps as the ones described in(Godat et al., 2012). Holes with a diameter of of 14 mm were drilled into the geometrical center of the concrete prism, thus grarateeing enough room for the epoxy adhesive. The bond between the CFRP rebar and the concrete was achived using an epoxy resin.

The experimental program was grouped into three series: SERIES 1, with a bond length, l_b, of 100 mm ($l_b = 14 \cdot t_f$); SERIES 2, with a bond length, l_b, of 200 mm ($l_b = 28 \cdot t_f$); and SERIES 3, with a bond length, l_b, of 300 mm ($l_b = 43 \cdot t_f$). The specimen length varied across the series, with lengths of 200 mm, 300 mm, and 400 mm for SERIES 1, SERIES 2, and SERIES 3, respectively. Figure 1a illustrates the geometry of each specimen, including the instrumentation employed.

Test set-up and instrumentation

The pull-out test configuration is depicted in Figure 1b. The tests were conducted using a servo-hydraulic testing machine with a maximum capacity of 300 kN. Displacement control was chosen to capture the post-peak behavior. The load was applied to the reinforcement bar at a rate of 0.02 mm/s and measured using a load cell with a maximum capacity of 300 kN and a linearity error of 0.05%. The displacements at the loaded and free ends were measured using two linear variable differential transformers (LVDTs), namely LVDT1 and LVDT2, respectively.

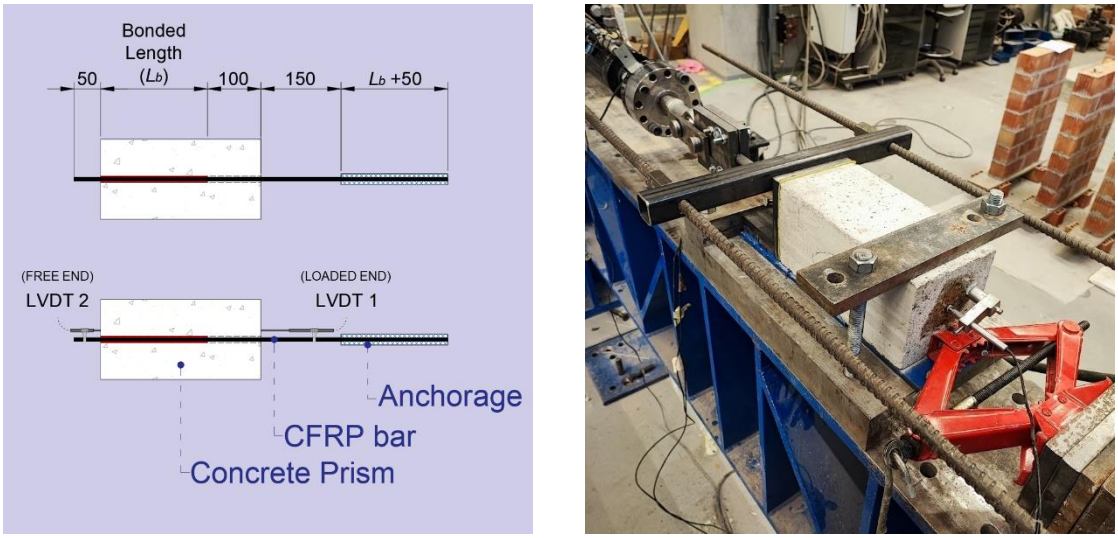

a) Specimen's geometry and instrumentation b) test setup

Figure 1: Specimen's geometry, instrumentation, and test set-up for direct pull-out tests.

Materials

The experimental study involved the use of concrete, CFRP bars, and a commercial cold-curing epoxy adhesive. The concrete employed had a compressive characteristic strength (cylinder/cube) of 30/37 MPa (C30/37) and belonged to exposure class XC4(P). It had a water/cement ratio of 0.40, maximum aggregate size of 12.5 mm, slump class S4 (slump of 160-210 mm), and was produced using Portland cement type CEM II/A-L 42.5R, in accordance with Eurocode 2 (CEN, 2004) standards. The modulus of elasticity (E_{cm}) and compressive strength (f_{cm}) of the concrete were evaluated using six cylindrical specimens with a diameter of 150 mm and height of 300 mm, following NP EN 12390-13:2013 (NP EN 12390-13, 2013) and NP EN 12390-3:2011 (NP, 2011) standards, respectively. The determined values were $E_{cm} = 26.6$ (CoV = 1.8%) GPa and $f_{cm} = 31.0$ (CoV = 5.7%) MPa, where CoV is the coefficient of variation.

The CFRP bars used in the investigation were prefabricated using a vacuum infusion method into a 7 mm thick plate. Subsequently, the CFRP plate was cut into 7 mm square bars using a water jet. The vacuum infusion method was chosen over the pultrusion method to enable the creation of non-linear geometries, aligning with the goals of the Sticker project. The tensile properties of the CFRP bars were assessed according to ISO 527-5:2009 (ISO, 1997). Six CFRP bar samples were tested, yielding the following main results: $E_f = 145.8$ (CoV = 5.1%) GPa and $f_f = 1462$ (CoV = 3.2%) MPa.

A commercial cold-curing epoxy adhesive was applied for connecting the CFRP bars to the concrete base. The supplier (S&P, 2018) reported that the adhesive's average elastic modulus surpassed 3,2 GPa. After seven days of curing at 20°C, this adhesive has a tensile strength of 15.9 MPa and a compressive strength of 104.4 MPa. In addition, following seven days of curing at 23°C, the glass transition temperature (Tg) is 53.5°C (S&P, 2018).

Interlaminar shear tests

Interlaminar shear tests were conducted alongside the direct pull-out tests to evaluate the interlaminar shear strength of the FRP composites. The tests followed the ISO 14130 standard, which employs the short-beam method to determine the apparent interlaminar shear strength of composites with thermoset or thermoplastic matrices. According to ISO 14130:1997, the test samples should have a total length of 10 times their height (70 mm in this study) and undergo a three-point bending test with a short span of 5 times their height (35 mm) under displacement control at a rate of 1 mm/min. To comply with these recommendations, the test setup shown in Figure 2a was utilized.

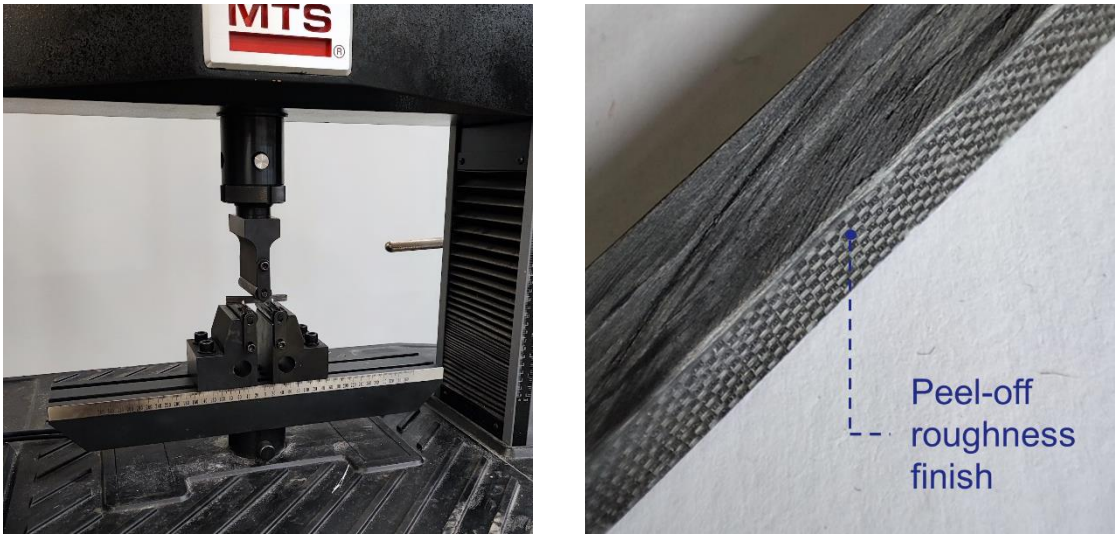

a) Test setup b) CFRP composits with peel-off finish

Figure 2: Interlaminary Shear test set up and detail of the peel-off roughness finish.

It is noteworthy that two types of CFRP laminates were prepared for the interlaminar shear tests: one with a peel-off roughness finish (as shown in Figure 2b) and another without any roughness treatment. Consequently, out of the 12 tested samples, 6 were from the peel-off composite (series PF), while the remaining 6 were from the composite without the peel-off finish (series NF). In addition to measuring the load and deflection, digital image correlation (DIC) was employed in this study to gain further insights into the stress distribution during the tests.

RESULTS AND DISCUSSION

Direct pull-out tests

The primary objective of this experimental study is to validate the effectiveness of CFRP composite bars produced through vacuum infusion as a reinforcement material for civil infrastructure. The influence of the bonded length is investigated while keeping all other variables constant throughout the tests. In the pull-out test, the stress distribution along the embedment length is non-uniform. Therefore, an average bond stress is defined as:

$$\tau = \frac{F}{p \cdot l_b} = \frac{F}{(4 \cdot w_f) \cdot l_b} \qquad \text{Eq. 1}$$

Here, F represents the tensile load, p is the perimeter of the rebar cross-section, and l_b is the embedment length. The bond behavior is analyzed by examining the relationship between the bond stress defined in Eq. 1 and the slip between the rebar and the concrete.

Table 1 presents the experimental results obtained from the bond tests, including the failure mode. In this table, τ_{max} represents the bond strength, and $s_{m,le}$ and $s_{m,ue}$ indicate the slip values at the bond strength for the loaded and free ends, respectively. The mean values of the bond strength and the corresponding slips for nominally identical specimens are also provided.

It is important to note that despite using a single concrete batch to produce the tested specimens, a normalized bond strength ${\tau_{max}}^*$ was calculated to account for the effect of concrete strength. This allowed for a meaningful comparison of the results with existing literature. The normalized bond strength ${\tau_{max}}^*$ was defined as follows:

$$ {\tau_{max}}^* = \frac{\tau_{max}}{\sqrt{f_{cm}}} \qquad \text{Eq. 2} $$

Where f_{cm} is the compressive strength of the concrete. By normalizing the bond strength, the influence of concrete strength variations among specimens can be accounted for, facilitating a fair comparison with other data available in the literature (Baena et al., 2009; Nepomuceno et al., 2021).

The results of the direct pull-out tests provide valuable insights into the behavior and performance of the CFRP composite bars produced by vacuum infusion for civil infrastructure reinforcement. The bond stress-slip relationship exhibited a distinctive global behavior characterized by an initial increase in bond stress with minimal slippage, followed by softening once the maximum bond stress was reached. Figure 3 illustrate the specimen curves for each tested bonded length, showcasing the variations in bond behavior.

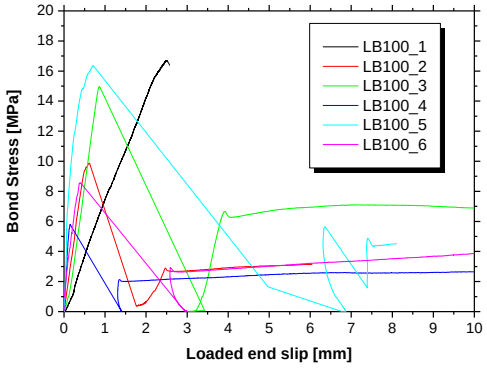

a) LB100 series

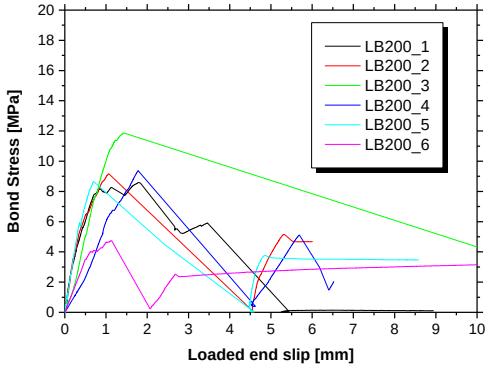

b) LB200 series

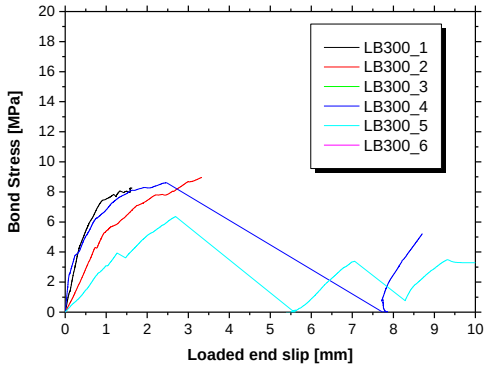

c) LB300 series

Figure 3: Bond stress *versus* Loaded end slip in the direct pull-out tests.

It is important to note that the slip values at the loaded end, as presented in Table 1 and Figure 3, have been adjusted to exclude the elastic deformation of the FRP bar. The elastic deformation was estimated by multiplying the strain of the FRP bar in the unbonded region (obtained from the relationship between force and elastic modulus) by the distance between the LVDT location and the beginning of the bonded region.

Within series LB100, LB200, and LB300, the maximum bond stresses (τ_{max}) were recorded as 12.05 MPa, 8.73 MPa, and 8.05 MPa, respectively. The corresponding slip values at the bond strength were 0.87 mm, 1.31 mm, and 0.61 mm for the loaded end ($s_{m,le}$), and 0.21 mm, 0.41 mm, and 0.61 mm for the free end ($s_{m,ue}$). Notably, the failure modes varied across the series. While the dominant failure mode was pull-out (PO) for most specimens, series LB200 and LB300 exhibited FRP failure in half of the specimens.

Table 1: Experimental results from direct pull-out tests

Series	Lable	F_{max} [kN]	τ_{max} [MPa]	${\tau_{max}}^{b}$ [MPa]	$s_{m,le}$ [mm]	${s_{m,le}}^{b}$ [mm]	$s_{m,ue}$ [mm]	${s_{m,ue}}^{b}$ [mm]	${\tau_{max}}^{*}$ [MPa]	$Failure\ Mode$
LB100	LB100_1	46.77	16.70	12.05	2.49	0.87	0.46	0.21	3.00	PO
	LB100_2	27.64	9.87		0.61		0.18		1.77	PO
	LB100_3	41.93	14.97		0.86		0.22		2.69	PO+FF
	LB100_4	16.25	5.80		0.14		0.00		1.04	PO
	LB100_5	45.80	16.36		0.71		0.29		2.94	PO
	LB100_6	23.98	8.57		0.40		0.10		1.54	PO
LB200	LB200_1	48.10	8.59	8.73	1.78	1.31	0.35	0.41	1.54	FF
	LB200_2	51.32	9.16		1.06		0.24		1.65	PO
	LB200_3	66.52	11.88		1.43		0.95		2.13	FF
	LB200_4	52.44	9.36		1.78		0.44		1.68	PO
	LB200_5	48.46	8.65		0.70		0.29		1.55	FF
	LB200_6	26.58	4.75		1.14		0.20		0.85	PO
LB300	LB300_1	69.40	8.26	8.05	1.60	2.02	0.69	0.61	1.48	FF
	LB300_2	75.25	8.96		3.33		(na)		1.61	FF
	LB300_3	(na)	(na)		(na)		(na)		(na)	(na)
	LB300_4	72.32	8.61		2.46		0.89		1.55	PO
	LB300_5	53.39	6.36		2.69		0.26		1.14	PO
	LB300_6	(na)	(na)		(na)		(na)		(na)	(na)

Notes: [b] Mean vaue for similar specimens; (na) specimen had to be disregarded due to thecnical problems in the acquisition system; Failure Mode: PO = Pullout, FF = FRP Failure

It is worth mentioning that the failure load for the FRP bars during these tests occasionally fell below the values obtained in the tensile characterization, which was 71.6 kN. This discrepancy can be attributed to the combined effect of tensile and shear stresses in the bar, leading to interlaminar shear failure. The presence of a bending moment on the bar during the test could have further contributed to this behavior. This finding is significant, as it suggests the possibility of premature failure in real-world applications of this CFRP bar, particularly in scenarios involving inclined and horizontal bars where normal, shear, and bending moments are present, especially at the transition between these sections.

Analyzing the bond stress-slip relationship, it is evident that an increase in bonded length resulted in a decrease of the τ_{max}. Although the average pull-out force was higher for longer bonded lengths, the τ_{max} did not increase proportionally. These curves exhibit a reduction in stiffness during the initial stage and a further reduction near the peak load. In contrast, series LB100 displayed a high initial stiffness and minimal change in stiffness leading to failure.

Moreover, even after pull-out failure occurred, a significant portion of the bond strength remained, with residual bond strengths approximately 40% of the maximum pull-out load for the majority of specimens.

Table 1 also presents the normalized bond strength $\tau_{max}{}^{*}$, which was used to comprare with results from the literature. In a study carried out by (Baena et al., 2009), 88 pull-out tests were conducted, which included several types of FRP types (glass, carbon) and geometries (diameter, and surface finish). The bond length was equal to 5 times de diameter of the bar, with bars diameters that ranged from 8 mm to 20 mm. The average normalized bond strength $\tau_{max}{}^{*}$ obtained in (Baena et al., 2009) investigation was equal to 2.57 MPa for the 88 specimens (included steel rebars) and equal to 2.39 MPa for specimens made with CFRP bars. In the same context, (Nepomuceno et al., 2021) presented a review on the bond between FRP bars and concrete, where from a database composed of 1002 pull-out test, an average normalized bond strength of 1.98 MPa was observed for CFRP rebars, whereas for Glass FRP (GFRP) and basalt FRP (BFRP) the normalized bond strength was 2.15 MPa and 2.77 MPa, respectively. As can be seen in Table 1, the average $\tau_{max}{}^{*}$ value obtained for series LB100, equal to 2.16 MPa, is within the values observed in the literature, which clearly indicates that this new composite performes adequatedly regarding the bond to concrete.

Interlaminar shear tests

The main results obtained from the interlaminar shear tests are summarized in Table 2, and the corresponding force versus displacement curves are illustrated in Figure 4. For the specimens with the peel-off finish (series PF), consistent results were observed, as indicated by the low coefficient of variation (CoV). These specimens exhibited an average interlaminar shear strength of 53.61 MPa. On the other hand, specimens from series NF displayed a slightly lower interlaminar shear strength of 45.78 MPa. The disparity in both the interlaminar shear strength values and the coefficient of variation between the two series suggests that the manufacturing process for the PF series specimens yielded better results. It is noteworthy that both series exhibited satisfactory outcomes, which were within the rage of values observed in the literatue for other FRP bars (Januš et al., 2022).

Table 2: Main results from the interlaminar shear tests

Surface	Specimen	F_{max} [kN]	δ_{max} [mm]	τ_{max} [MPa]	Failure Mode
With the Peel-off roughness Finish (PF series)	PF_1	3.52	0.81	53.95	MSF
	PF_2	3.55	0.79	54.41	MSF
	PF_3	3.37	0.76	51.55	MSF
	PF_4	3.44	0.80	52.63	MSF
	PF_5	3.59	0.79	54.93	MSF
	PF_6	3.54	0.77	54.16	MSF
	Mean	3.50	0.79	53.61	
	CoV	2.1%	2.2%	2.2%	
Without the peel-off roughness finish (NF Series)	NF_1	2.45	0.62	37.58	MSF
	NF_2	3.14	1.19	48.04	SSF
	NF_3	2.91	1.05	44.54	SSF
	NF_4	2.65	0.89	40.55	MSF
	NF_5	3.36	0.69	51.41	MSF
	NF_6	3.43	0.89	52.55	MSF
	Mean	2.99	0.89	45.78	
	CoV	12.0%	22.0%	11.9%	
Notes: Failure Mode: MSF = multiple shear failure, SSF = single shear failure					

Upon examining the force versus displacement curves in Figure 4, it is evident that series NF exhibited a higher dispersion in results compared to series PF. It should be emphasized that both series exhibited similar behavior, with an initial linear stage up to the peak load, followed by a post-peak stage where the load gradually decreased with increasing deflection.

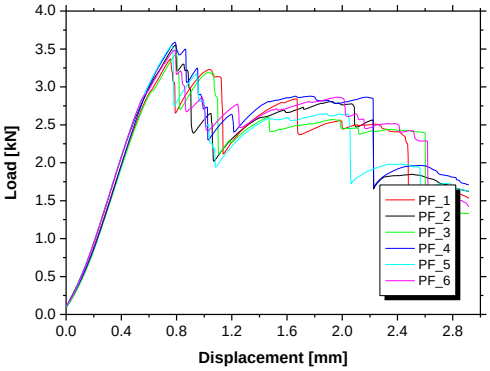

a) CFRP composits with peel-off finish

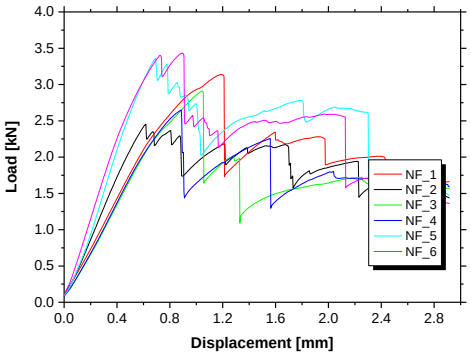

b) CFRP composits without peel-off finish

Figure 4: Load *versus* displacement in the interlaminary Shear tests.

All specimens from series PF exhibited a multiple shear failure (MSF) mode. Similarly, the specimens from series NF predominantly demonstrated MSF as the failure mode, although two specimens exhibited single shear failure (SSF). Figure 5a presents the tested specimens, while a detailed view of the MSF failure mode is depicted in Figure 5b.

a) Tested specimens

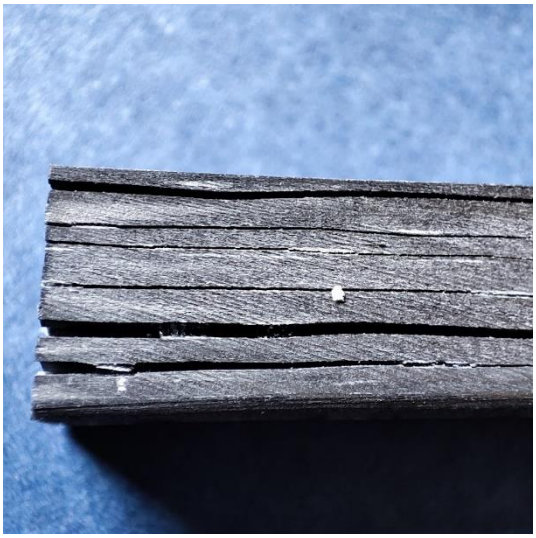

b) multiple shear failure (detail)

Figure 5: Failure modes in the interlaminary Shear tests.

In order to complement the experimental investigation, finite element (FE) analysis was conducted to simulate the interlaminar shear tests. The following methodology was employed for the FE analysis: A cohesive element with a thickness of 0.005 mm was utilized to model the interfacial behavior between the layers. To reduce computational time, half of the specimen was modeled due to the symmetry of the interlaminar shear test setup. Four different models were created to explore the influence of laminate configuration: (1) a model with two (meso) layers, each 3.5 mm thick, (2) a model with three layers of 2.3 mm each, (2) a model with five layers of 1.4 mm each, and (3) a model with seven layers of 1 mm each. Figure 6 ilustrates the bondary conditions, and FE mesh used for the simulation of the interlaminar shear tests.

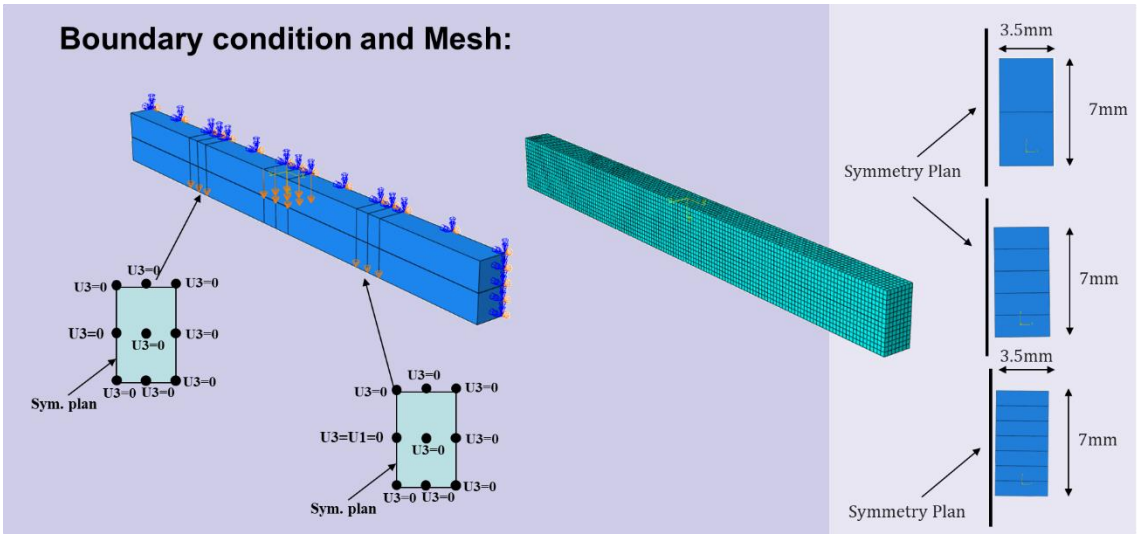

Figure 6: Model geometry, boundary conditions and mesh

The maximum mesh size was set to 0.5 mm for the analysis. The CFRP elements were modeled using the SC8R element type, which is an 8-node quadrilateral in-plane continuum shell with finite membrane strains. The cohesive elements were represented using the COH3D8 element type, an 8-node three-dimensional cohesive element.

The CFRP material was modeled using an Elastic Lamina with the Hashin damage model. The cohesive material was modeled using the Quadratic nominal stress damage initiation criteria and the Benzeggagh-Kenane (BK) damage evolution criteria (Benzeggagh & Kenane, 1996). The elastic parameters and Hashin parameters for the CFRP material and Cohesive material were assigned based on the values provided in Table 3.

Fracture energies were assigned to the CFRP and cohesive materials for both mode I (G_{IC}) and mode II (G_{IIC}). For mode I fracture, the CFRP material had a fracture energy of 0.4 N/mm, while the cohesive material had a fracture energy of 0.6 N/mm. For mode II fracture, the CFRP material had a fracture energy of 0.6 N/mm, and the cohesive material had a fracture energy of 1.0 N/mm.

Table 3: Material parameters used for FEM analysis

CFRP material				Cohesive material			
Elastic Parameters		Hashin parameters		Elastic Parameters		Damage Parameters	
E_1 [MPa]	94100	σ_A^+ [MPa]	1500	E [MPa]	2600	S_n [MPa]	35
E_2 [MPa]	1500	σ_A^- [MPa]	800	G_1 [MPa]	929	S_{t1} [MPa]	60
υ [-]	0.28	σ_T^+ [MPa]	330	G_2 [MPa]	929	S_{t2} [MPa]	60
G_{12} [MPa]	6000	σ_T^- [MPa]	500	υ [-]	0.4		
G_{13} [MPa]	6000	τ_T [MPa]	90				
G_{23} [MPa]	4000	τ_A [MPa]	53.56/47.46				
Notes: E_1 – Longitudinal modulus of elasticity; E_2 – Transverse modulus of elasticity; υ – Poisson's ratio; $\{G_{12}, G_{13}, G_{23}\}$ – Shear modulus; σ_A^+ – Longitudinal tensile strength; σ_A^- – Longitudinal compressive strength; σ_T^+ – Transverse tensile strength; σ_T^- – Transverse compressive strength; τ_T – Transverse shear strength; τ_A – Longitudinal shear strength; E –Modulus of elasticity; $\{G_1, G_2\}$ – Shear modulus; S_n – Normal stress for damage initiation; and $\{S_{t1}, S_{t2}\}$– Shear stress for damage initiation.							

The results indicated that increasing the number of meso-layers improved the agreement between the maximum load obtained from the analysis and the experimental results. With the inclusion of three meso-layers, the failure mode was accurately predicted, exhibiting total debonding of the bottom layer and a single shear failure mode. With five and seven Meso-layers, both configurations successfully predicted the failure mode observed in the experiments. Figure 7 presents a comparison between the average load versus displacement curve obtained experimentally with the PF specimens, and the FEM model with 5 meso layers. As can be seen, there is a good agreement between the experimental results and the FEM simulation, with identical peak load achived in the FEM and a progressive load decrease caused by the failure between the meso layers due to the shear stress.

This FEM analysis showed that the damage initiation stress in the shear direction and the damage evolution parameters of the cohesive material controlled the maximum load and the post-peak behavior of the specimens. Also, by increasing the cohesive strength and damage evolution parameters it was possible to obtain better predictions in terms of maximum load, however the failure mode did not match the experimental results.
The FE analysis provided valuable insights into the interlaminar shear behavior of the laminates, highlighting the importance of laminate configuration and cohesive material properties in determining the maximum load, failure mode, and post-peak behavior.

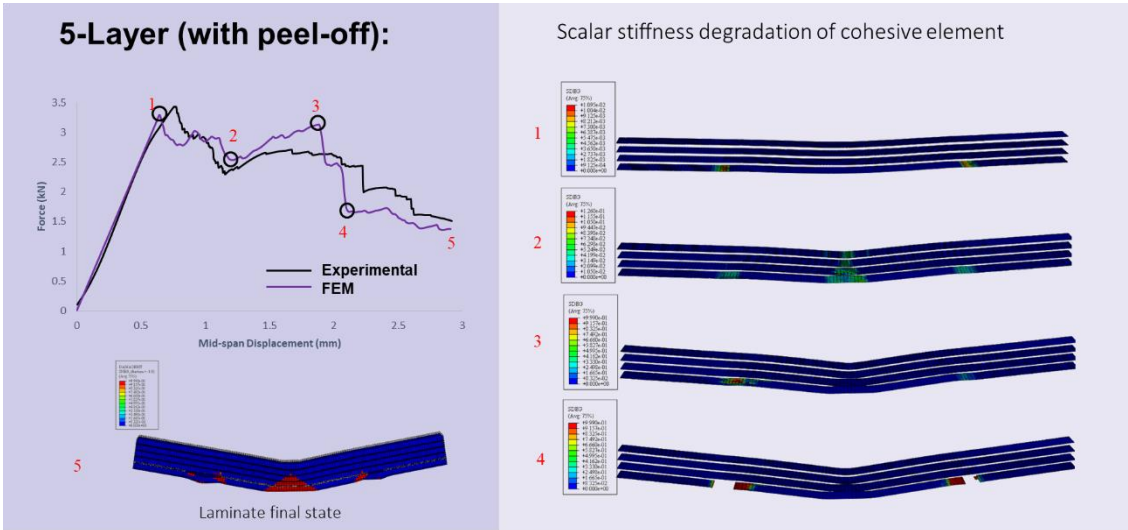

Figure 7: Comparison between the experimental results (series PF) and the FEM model with 5 meso layers.

CONCLUSION

In this paper, the performance of a new generation of CFRP bars adhesively bonded to concrete were evaluated by the use of direct pull-out tests (DPT). Furthermore, the interlaminar shear tests were conducted to deeply evaluate the composites mechanical properties. Based on the main results and discussion presented, the following conclusions can be drawn:

- The pull-out tests revealed a non-linear relationship between the bond stress and loaded end slip, characterized by an initial increase in bond stress followed by softening after reaching the maximum bond stress. The bond performance was influenced by the bonded length, with a decrease in pull-out stress observed as the bonded length increased.
- The failure modes on the DPT varied between pull-out and FRP failure. In some cases, the FRP failure load during the pull-out tests was lower than the tensile characterization load, primarily due to the combined effect of tensile and shear stresses in the CFRP bars, resulting in interlaminar shear failure.

- The interlaminar shear tests provided valuable insights into the structural integrity of the composite material. In these tests, multiple shear failure was the dominant failure mode. Two series were tested, with a better performance from the PF series, with a peel-off finish, which showed higher interlaminar shear strength and lower result dispersion. Thus indicating that the manufacturing process with the peel-off finish yield to better composite solution. Both series did, nevertheless, performed adequadly, with the results being within the range of values available in the literature.
- The FEM analysis on the interlaminar tests revealed that the number of meso-layers in the laminate influenced the maximum load and failure mode. Increasing the number of meso-layers improved the agreement between the predicted maximum load and experimental results. For laminates with three meso-layers, the failure mode was characterized by total debonding of the bottom layer and single shear failure. Laminates with five and seven meso-layers exhibited proper failure modes and predicted behavior. The maximum load and post-peak behavior were predominantly controlled by the damage initiation stress in the shear direction and the damage evolution parameters of the cohesive material.

ACKNOWLEDGEMENT

This article is based upon work from COST Action CA18120 (CERTBOND - https://certbond.eu/), supported by COST (European Cooperation in Science and Technology). This study is also a part of the project ‘‘Sticker –Innovative technique for the structural strengthening based on using CFRP laminates with multifunctional attributes and applied with advanced cement adhesives’’, with the reference POCI-01-0247-FEDER-039755. This work was partly financed by FCT / MCTES through national funds (PIDDAC) under the R&D Unit Institute for Sustainability and Innovation in Structural Engineering (ISISE), under reference UIDB/04029/2020, and under the Associate Laboratory Advanced Production and Intelligent Systems ARISE under reference LA/P/0112/2020.

CONFLICT OF INTEREST

The authors declare that they have no conflicts of interest associated with the work presented in this paper.

DATA AVAILABILITY

Data on which this paper is based is available from the authors upon reasonable request.

REFERENCES

Baena, M., Torres, L., Turon, A., & Barris, C. (2009). Experimental study of bond behaviour between concrete and FRP bars using a pull-out test. *Composites Part B: Engineering*, *40*(8), 784–797. https://doi.org/10.1016/j.compositesb.2009.07.003

Barros, J. A. O., Figueiredo, F. P., Costa, I. G., & Dourado, F. N. F. M. (2022). New type of CFRP reinforcement and technique for the flexural strengthening of RC balconies. *Composite Structures*, *280*, 114899. https://doi.org/10.1016/j.compstruct.2021.114899

Barros, J. A. O., & Fortes, A. S. (2005). Flexural strengthening of concrete beams with CFRP laminates bonded into slits. *Cement and Concrete Composites*, *27*(4), 471–480. https://doi.org/10.1016/j.cemconcomp.2004.07.004

Barros, J. A. O., Rezazadeh, M., Laranjeira, J. P. S., Hosseini, M. R. M., Mastali, M., & Ramezansefat, H. (2017). Simultaneous flexural and punching strengthening of RC slabs according to a new hybrid technique using U-shape CFRP laminates. *Composite Structures*, *159*, 600–614. https://doi.org/https://doi.org/10.1016/j.compstruct.2016.10.009

Barros, J., Rezazadeh, M., Costa, I., Baghi, H., Hosseini, M. R. M., Mastali, M., & Laranjeira, J. (2016). Flexural and shear/punching strengthening of RC beams/slabs using hybrid NSM-ETS

technique with innovative CFRP laminates. In Z. A. (Ed.), *6th International Conference on Structural Engineering, Mechanics and Computation, SEMC 2016* (pp. 1500–1505). CRC Press/Balkema. https://doi.org/10.1201/9781315641645-246

Benzeggagh, M. L., & Kenane, M. (1996). Measurement of mixed-mode delamination fracture toughness of unidirectional glass/epoxy composites with mixed-mode bending apparatus. *Composites Science and Technology*, *56*(4). https://doi.org/10.1016/0266-3538(96)00005-X

Carlos Augusto Nonato da Silva. (2019). *Analytical and numerical models for simulating the mechanical behaviour of discrete and continuous reinforcements in cracked cement composites*. University of Rome.

CEN. (2004). *CEN EN 1992-1-1 European Standard Eurocode 2: Design of concrete structures - Part 1-1: general rules and rules for buildings*.

Chalioris, C., Kosmidou, P.-M., & Papadopoulos, N. (2018). Investigation of a New Strengthening Technique for RC Deep Beams Using Carbon FRP Ropes as Transverse Reinforcements. *Fibers*, *6*(3), 52. https://doi.org/10.3390/fib6030052

Dias, S. J. E., Silva, J. R. M., & Barros, J. A. O. (2021). Flexural and shear strengthening of reinforced concrete beams with a hybrid CFRP solution. *Composite Structures*, *256*, 113004. https://doi.org/https://doi.org/10.1016/j.compstruct.2020.113004

Firmo, J. P., Correia, J. R., & Bisby, L. A. (2015). Fire behaviour of FRP-strengthened reinforced concrete structural elements: A state-of-the-art review. *Composites Part B: Engineering*, *80*, 198–216. https://doi.org/https://doi.org/10.1016/j.compositesb.2015.05.045

Godat, A., L'Hady, A., Chaallal, O., & Neale, K. W. (2012). Bond Behavior of the ETS FRP Bar Shear-Strengthening Method. *Journal of Composites for Construction*, *16*(5), 529–539. https://doi.org/10.1061/(asce)cc.1943-5614.0000280

Imjai, T., Garcia, R., Guadagnini, M., & Pilakoutas, K. (2020). Strength Degradation in Curved Fiber-reinforced Polymer (FRP) Bars Used as Concrete Reinforcement. *Polymers*, *12*(8), 1653. https://doi.org/10.3390/polym12081653

ISO, N. P. E. N. (1997). *ISO 527-5:1997 - Plastics -- Determination of tensile properties Part 5.pdf*.

Januš, O., Girgle, F., Rozsypalová, I., Kostiha, V., Prokeš, J., Štěpánek, P., & Čairović, Đ. (2022). Influence of test parameters on the interlaminar shear strength of FRP bars. *Composite Structures*, *299*, 116061. https://doi.org/10.1016/j.compstruct.2022.116061

Kaya, E., Kütan, C., Sheikh, S., & İlki, A. (2017). Flexural Retrofit of Support Regions of Reinforced Concrete Beams with Anchored FRP Ropes Using NSM and ETS Methods under Reversed Cyclic Loading. *Journal of Composites for Construction*, *21*(1), 4016072. https://doi.org/10.1061/(ASCE)CC.1943-5614.0000732

Nepomuceno, E., Sena-Cruz, J., Correia, L., & D'Antino, T. (2021). Review on the bond behavior and durability of FRP bars to concrete. *Construction and Building Materials*, *287*. https://doi.org/10.1016/j.conbuildmat.2021.123042

Nonato Da Silva, C. A., Ciambella, J., Barros, J. A. O., & Costa, I. G. (2019). Analytical bond model for general type of reinforcements of finite embedment length in cracked cement based materials. *International Journal of Solids and Structures*, *167*, 36–47. https://doi.org/10.1016/j.ijsolstr.2019.02.018

NP. (2011). *EN 12390-3: Testing hardened concrete. Part 3: Compressive strength of test specimens*.

NP EN 12390-13. (2013). Ensaios do betão endurecido - Part 13: Determinação do Modulo de elasticidade secante à compressão. *IPQ - Instituto Portugues Da Qualidade*.

S&P. (2018). *Technical Data Sheet S & P Resin 55 HP epoxy adhesive*. 1–3.

Teng, J. G., Lorenzis, L. De, Wang, B., Li, R., Wong, T. N., & Lam, L. (2006). Debonding Failures of RC Beams Strengthened with Near Surface Mounted CFRP Strips. *Journal of Composites for Construction*, *10*(2), 92–105. https://doi.org/10.1061/(ASCE)1090-0268(2006)10:2(92)